



Electromechanical dynamic simulation and experiment for multi-stage gear transmission system with planetary gears

Yong Wang^{1,2} · Changzhao Liu¹ · Yinghua Liao^{1,3}

Received: 4 December 2017 / Revised: 9 January 2018 / Accepted: 11 January 2018 / Published online: 30 January 2018
© Springer Science+Business Media, LLC, part of Springer Nature 2018

Abstract

A large number of machineries, such as long-wall shearer and tunnel boring machine, contain the multi-stage gear transmission system with planetary gears driven by electric motor, whose electromechanical characteristics have significant effect on the performance of machineries. Therefore, a test rig of this kind of transmission system is established, and the electromechanical dynamic model is also constructed for it, including the electric motor and the gear transmission. Moreover, to obtain more accurate simulation results, a method is proposed to estimate the equivalent damping value of the gear transmission system in the aspect of energy based on the testing data. Next, the electromechanical dynamic characteristics, including the motor current and the internal load of the gear transmission, are investigated by experiment and simulation under shock and step load to provide some guidance for improving the dynamic performance and monitoring the working state. The electromechanical dynamic modeling method is also well validated by the comparison between the simulating and test results.

Keywords Multi-stage gear transmission system · Planetary gears · Electromechanical dynamic characteristics · Simulation · Experiment

1 Introduction

The multi-stage gear transmission system with planetary gears driven by electric motor, as shown in Fig. 1, is always used by all kinds of machinery, such as long-wall shearer, tunnel boring machine, and so on. The electric motor that can adjust speed, such as direct torque control (DTC) induction motor, is always chosen as the power source. Generally, this kind of transmission system usually works under the condition of sudden-changing loads, therefore, it is essential to conduct an electromechanical dynamic investigation under sudden-changing load by simulation and experiment, which can provide some guidance for improving the dynamic performance and monitoring the working state.

Using the cutting transmission system on the long-wall shearer as an example, to construct the electromechanical dynamic model of the cutting transmission system under sudden-changing load, three parts of models are needed, including the model of DTC induction motor, dynamic model of gear transmission system, and drum (flywheel) load model. The model of DTC induction motor is depicted in detail in reference [1], so this model is used directly herein. The sudden-changing drum load can be represented by pulse and step load. The dynamic models of gear transmissions will be introduced following in detail.

The rotating speed of the transmission system is usually variable, and the generalized coordinate of the rotor in the electric motor model is the angular displacement, so a dynamic model of variable speed process for the gear transmission system is needed, with the angular displacements being chosen as generalized coordinates to be connected with the electric motor model conveniently.

The gear transmission system contains the parallel-axis gears and planetary gear set. Many dynamic models have been proposed for parallel-axis gears [2–4] and planetary gears [5–8]. These models are proposed to mainly investigate the vibration properties of gear transmission systems, moreover, the vibratory translational and angular displacements

✉ Changzhao Liu
czliu@cqu.edu.cn

¹ State Key Laboratory of Mechanical Transmission, Chongqing University, Chongqing 400044, China

² Department of Automotive Engineering, Chongqing College of Electronic Engineering, Chongqing 401331, China

³ Sichuan Provincial Key Lab of Process Equipment and Control, Sichuan University of Science & Engineering, Zigong, Sichuan 643000, China

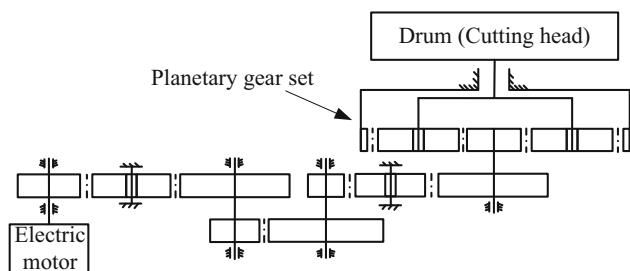


Fig. 1 The multi-stage gear transmission system with planetary gears on the long-wall shearer

are usually chosen as general coordinates. Therefore, these models just can be used in vibration analysis of transmission systems at a stable rotating speed with small fluctuation, not for variable speed processes. Moreover, it is not convenient to connect these gear dynamic models to the motor model, because the generalized coordinate of rotor is angular displacement in the motor model. Therefore, in this investigation, the dynamic model of variable speed process for parallel-axis gears [9] and planetary gears [10] are used to construct the dynamic model of the gear transmission systems. The dynamic model [9] is proposed for herringbone gears during the non-stationary process and considers the teeth friction, but it is easy to be simplified to torsional dynamic model of spur gears. The dynamic model [10] is proposed for spur planetary gear set during the non-stationary process, which is simplified from the translational-torsional dynamic model of variable speed process for the herringbone planetary gear set in the reference [11]. Therefore, the dynamic model of the gear transmission of the study herein chooses the angular displacements as the generalized coordinates, moreover, the meshing stiffness is variable with the angular displacements of gears. As a result, this model can be used in non-stationary process and is convenient to be connected to the electric motor model to construct the electromechanical dynamic model.

Some simulations have been conducted for the electromechanical dynamic analysis of the motor-gear system in previous literature [12–18], but in these simulations, the electric motor is not controlled. The steady-state model of electric motor is utilized [12–15], while [16–18] the dynamic model

of electric motor is utilized. These studies [13–18] mostly focus on the parallel-axis gear pairs. The dynamic model of the planetary gear set [12] is constructed based on these models [6, 19, 20] by modifying the meshing stiffness according to the mean angular velocity. The variation of the mean rotating speed must be determined in advance, while, most of time, the rotating speed is usually unknown before the electromechanical dynamic model is simulated especially when the dynamic electric motor model is utilized.

In this study, a test rig of the multi-stage gear transmission system with planetary gears is established firstly, and then, the electromechanical dynamic model is constructed for the experimental transmission system including the DTC induction motor, gear transmission, flywheel load. To obtain more accurate simulation results, a method is proposed to estimate the equivalent damping value of the gear transmission system in the aspect of energy based on the testing data. Next, the electromechanical dynamic characteristics are investigated by experiment and simulation under shock and step load to provide some guidance for improving the dynamic performance and monitoring the working state. Moreover, the comparison between the simulating and testing results is also conducted to validate the electromechanical dynamic modeling method herein.

2 Brief introduction to test rig of the multi-stage gear transmission system

The overall scheme of the test rig is shown in Fig. 2. Three main parts are contained in test rig, including the power source, gear transmission system, and loading equipment. The power source is composed of the DTC converter and electric motor. The gear transmission system is composed of a two-stage parallel-axis gear reducer and a planetary gear reducer. The loading equipment is composed of a dynamometer, an increasing gearbox, and a torque/speed transducer. The torque/speed transducer 1 is used to measure the input torque/speed of parallel-axis gear reducer to estimate the dynamic meshing force of the high speed stage of parallel-axis gear reducer. The torque/speed transducer 2 is used to

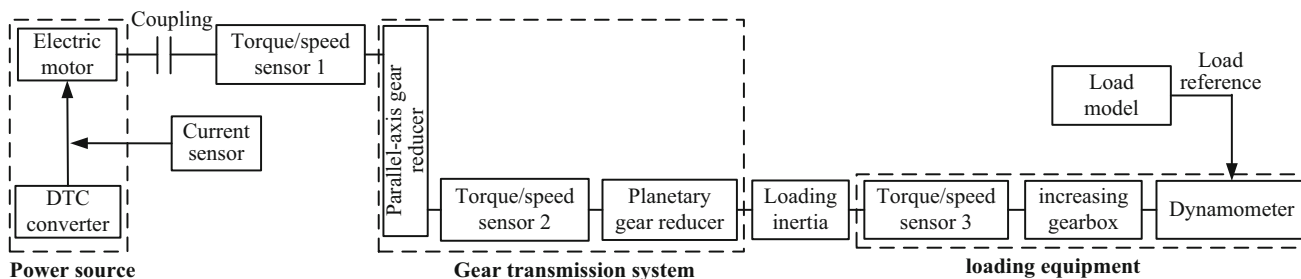
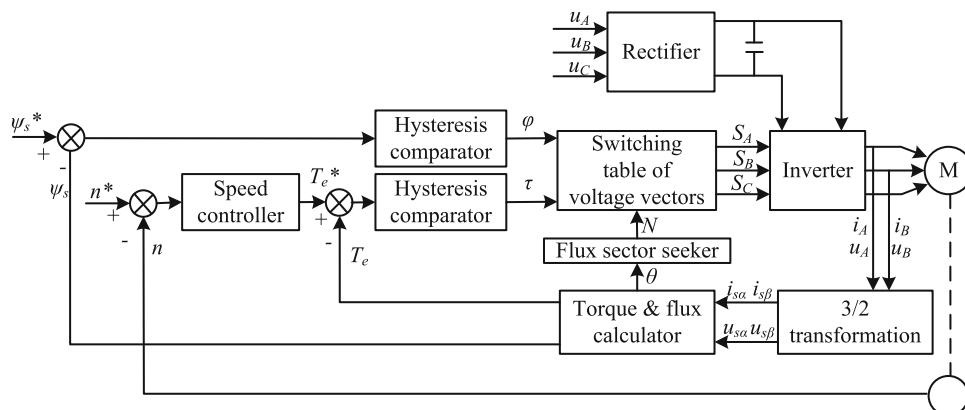


Fig. 2 Overall scheme of the test rig

Fig. 3 Photo of the test rig



Fig. 4 Control block diagram of the DTC induction motor



measure the input torque/speed of the planetary gear set to estimate the dynamic meshing force of the sun-planet gear pair of the planetary gear set. The torque/speed transducer 3 is used to measure the realistic flywheel load and speed. The Photo of the test rig is shown in Fig. 3.

3 Electromechanical dynamic model of the multi-stage gear transmission system

To construct the electromechanical dynamic model of the multi-stage gear transmission system under sudden-changing load, three parts of models are needed, including the model of DTC induction motor, dynamic model of the mechanical part (gear transmission system and flywheel), and load model. The sudden-changing load can be represented by pulse and step load, so just the models of DTC induction motor and mechanical part are introduced following in detail. How to combine these models to form the electromechanical dynamic model of the multi-stage gear transmission system is also introduced.

3.1 Model of DTC induction motor

In this study, the DTC induction motor is chosen as the power source of the multi-stage gear transmission system. The induction motor is controlled as shown [1] where the stator flux is circular. The control block diagram of the DTC induction motor is shown in Fig. 4. The flux ψ_s , torque T_e , and angle of the flux θ can be obtained from the block “torque & flux calculator” with the stator current (i_A, i_B) and voltage

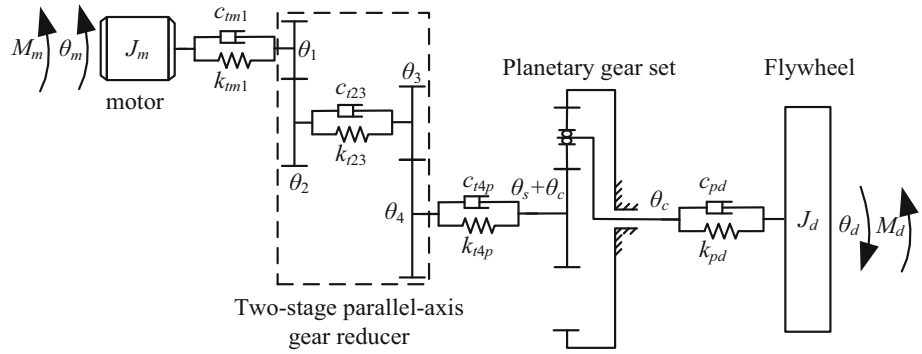
(u_A, u_B) signals. The ψ_s and T_e are compared with the given flux ψ_s^* and Torque T_e^* to obtain the signal φ and τ to decide the flux and torque decrease or increase. The signal of sector number N can be obtained by the block “flux sector seeker” with signal of θ . Then, the switching signals of (S_A, S_B , and S_C) are decided by φ, τ , and N with the block “switching table of voltage vectors” to control the inverter providing appropriate voltage vectors for the induction motor.

3.2 Dynamic model of the mechanical part

The torsional dynamic model of the mechanical part of the multi-stage gear transmission system is shown in Fig. 5, and the mathematical model is derived as Eq. (1). The dynamic model of parallel-axis gears used herein is torsional model that is simplified from the translational-torsional dynamic model of variable speed process for herringbone gears in the reference [9]. The dynamic model of the planetary gear set is the torsional model which proposed in the reference [10]. The generalized coordinate of the dynamic model of the mechanical part is angular displacement, so it is convenient to be connected to the model of DTC induction motor for electromechanical dynamic model of the experimental cutting transmission system.

In Eq. (1), the symbols $J_m, J_1, J_2, J_3, J_4, J_s, J_r, J_c$ and J_{pn} are rotational inertias of motor rotor, gear 1, gear 2, gear 3, gear 4, sun, ring, carrier, and the n th planet respectively; the symbols $\theta_m, \theta_1, \theta_2, \theta_3, \theta_4, \theta_s, \theta_r, \theta_c$ and θ_{pn} are angular displacements of motor rotor, gear 1, gear 2, gear 3, gear 4, sun, ring, carrier, and the n th planet respectively, and the θ_s, θ_r , and θ_{pn} are measured in the moving coordinate system;

Fig. 5 Dynamic model of the mechanical part of the multi-stage gear transmission system



the symbols $r_{b1}, r_{b2}, r_{b3}, r_{b4}, r_{bs}, r_{br}$, and r_{bpn} are radii of base circle of gear 1, gear 2, gear 3, gear 4, sun, ring, and the n th planet respectively, and r_{bc} is radius of distribution circle of planets; α_s and α_r are meshing angles of sun-planet and planet-ring gear pair respectively; $F_{y12}, F_{y34}, F_{Eyn}$, and F_{Iyn} are meshing forces of gear 1-2, gear 3-4, the n th sun-planet and planet-ring gear pairs respectively; The calculations of F_{y12} and F_{y34} are depicted in the reference [9], and the calculations of F_{Eyn} , and F_{Iyn} are depicted in the reference [10]; $k_{tm1}, k_{t23}, k_{t4p}$, and k_{pd} are torsional stiffness of motot-gear 1, gear 2-3, gear 4-planetary gear set, planetary gear set-flywheel respectively; $c_{tm1}, c_{t23}, c_{t4p}$, and c_{pd} are torsional damping of motor-gear 1, gear 2-3, gear 4-planetary gear set, planetary gear set-flywheel respectively; it is rigid connection between gear 2 and gear 3, as well as between the planetary gear set and flywheel, so c_{t23} and c_{pd} are set to be zero in the simulation herein; c_{tm1} contains the damping of the coupling after the motor and the equivalent damping of the parallel-axis gear reducer; c_{t4p} is the equivalent damping of the planetary gear reducer; the equivalent damping of the parallel-axis gear reducer and planetary gear reducer can be estimated by testing data in the aspect of energy that will be introduced in Sect. 3.3; η_{14} , and η_{sd} are efficiencies from gear 1 to 4 and from planetary gear to flywheel respectively, that can be obtained from the test data or handbook.

$$\begin{cases}
 J_m \ddot{\theta}_m + [k_{tm1}(\theta_m - \theta_1) + c_{tm1}(\dot{\theta}_m - \dot{\theta}_1)] / \eta_{14} = M_m \\
 J_1 \ddot{\theta}_1 - k_{tm1}(\theta_m - \theta_1) - c_{tm1}(\dot{\theta}_m - \dot{\theta}_1) + F_{y12}r_{b1} = 0 \\
 J_2 \ddot{\theta}_2 - F_{y12}r_{b2} + k_{t23}(\theta_2 - \theta_3) + c_{t23}(\dot{\theta}_2 - \dot{\theta}_3) = 0 \\
 J_3 \ddot{\theta}_3 - k_{t23}(\theta_2 - \theta_3) - c_{t23}(\dot{\theta}_2 - \dot{\theta}_3) + F_{y34}r_{b3} = 0 \\
 J_4 \ddot{\theta}_4 - F_{y34}r_{b4} + [k_{t4p}(\theta_4 - \theta_s - \theta_c) \\
 + k_{t4p}(\dot{\theta}_4 - \dot{\theta}_s - \dot{\theta}_c)] / \eta_{sd} = 0 \\
 J_d \ddot{\theta}_d - k_{t4p}(\theta_c - \theta_d) - c_{t4p}(\dot{\theta}_c - \dot{\theta}_d) = -M_d \\
 J_s(\ddot{\theta}_s + \ddot{\theta}_c) - k_{t4p}(\theta_4 - \theta_s - \theta_c) - c_{t4p}(\dot{\theta}_4 - \dot{\theta}_s - \dot{\theta}_c) \\
 - \sum_{n=1}^N F_{Eyn}r_{bs} = 0 \\
 J_r(\ddot{\theta}_r + \ddot{\theta}_c) + k_{\theta r}(\theta_r + \theta_c) - \sum_{n=1}^N F_{Iyn}r_{br} = 0 \\
 J_c \ddot{\theta}_c + c_{t4p}(\dot{\theta}_c - \dot{\theta}_d) + k_{t4p}(\theta_c - \theta_d) \\
 + \sum_{j=1}^N (F_{Eyn} \cos(\alpha_s) + F_{Iyn} \cos(\alpha_r))r_c = 0 \\
 J_{pn} \ddot{\theta}_{pn} - (F_{Eyn}r_{bpn} - F_{Iyn}r_{bpn}) = 0
 \end{cases}
 \tag{1}$$

3.3 Estimation of the torsional damping

The equivalent damping of parallel-axis reducer and planetary gear reducer is not from the realistic damper, but it describes the synthetical dissipation effect of vibratory energy for the reducer. The equivalent damping is caused by all the factors that can dissipate energy, for example, bearing friction, teeth friction [9], lubrication [21], contact deformation [22], churning [23], and so on, so it is difficult to calculate the equivalent damping value by a simple theoretical formula. Therefore, a method is proposed herein to estimate the equivalent damping value in the aspect of energy based on the testing data. This method is introduced by an example of a pair of gears as shown in Fig. 6. The pair of gears can be equal to a springoscillator as shown in Fig. 7. The effect of damping is mainly to dissipate the vibration of gears, so the damping can be estimated by the principle that the energy dissipated by the equivalent damping is equal to the vibratory energy loss between the input and output ends.

The torque fluctuation of the input end:

$$\delta T_1 = T_1 - T_{m1} \tag{2}$$

The speed fluctuation of the input end:

$$\delta \omega_1 = \omega_1 - \omega_{m1} \tag{3}$$

The torque fluctuation of the output end:

$$\delta T_2 = T_2 - T_{m2} \tag{4}$$

The speed fluctuation of the output end:

$$\delta \omega_2 = \omega_2 - \omega_{m2} \tag{5}$$

The relative speed of the output to the input end

$$\delta \omega_{21} = i \cdot \delta \omega_2 - \delta \omega_1 \tag{6}$$

Based on the principle that the energy dissipated by equivalent damping is equal to the vibratory energy loss between

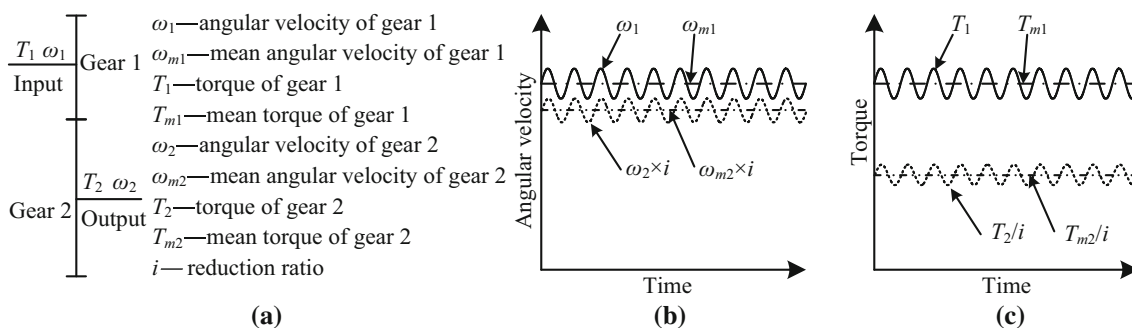


Fig. 6 Input and output angular velocity (b) and torque (c) of a pair of gears (a)

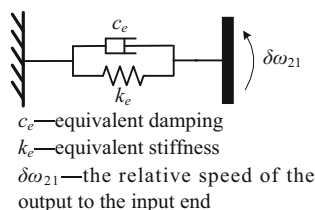


Fig. 7 Equivalent torsional spring oscillator of gears

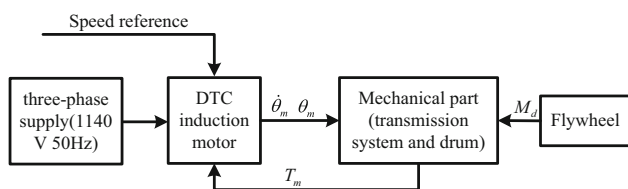


Fig. 8 Relationship between models of the DTC motor, mechanical part and flywheel of the multi-stage gear transmission system

the input and output ends, the calculation of the equivalent damping can be derived as Eq. (7):

$$c_e = \frac{\text{rms}(\delta T_2 \cdot \delta \omega_2) - \text{rms}(\delta T_1 \cdot \delta \omega_1)}{\text{rms}(\delta \omega_{21} \cdot \delta \omega_{21})} \quad (7)$$

In Eq. (7): “rms” is the function of root mean square. The fluctuations of torque and speed like alternating current, so the work did by the fluctuating torque and speed is calculated by “rms”.

3.4 Construction of the electromechanical dynamic model

Figure 8 gives the relationship between models of the DTC motor, mechanical part and flywheel of the multi-stage gear transmission system of the long-wall shearer. The electromechanical dynamic model of the multi-stage gear transmission system can be constructed by the relationship.

4 Electromechanical dynamic simulation and experiment

The multi-stage gear transmission system is shown in Fig. 3. The parameters of the cutting transmission for simulation are shown in Table 1. The load on the flywheel used in the simulation is obtained from the measuring results of torque/speed transducer 3.

4.1 Investigation under the shock load

The shock flywheel load is shown in Fig. 9, which is obtained from the measuring results of torque/speed transducer 3. The flywheel load at stable period contains two frequency components of 9.9 and 48.3 Hz as shown in Fig. 9b. At the beginning of the simulation, it is the transient process, so the simulating result of 0.9 ~ 3.4 s is chosen to be compared with the test result.

The current characteristics of test and simulation are given in Fig. 10. In Fig. 10a, the flywheel load and stator current of test are compared in time domain. The stator current is RMS current, the same below. After the shock load is acted, the stator current increases. The stator can reflect the sudden change of the flywheel load but with a little delay. In Fig. 10b, the stator currents of test and simulation are compared in time domain. For clarification of the illustration, the stator currents are low-pass filtered with cutting frequency of 20 Hz. The variation trend of the stator current of simulation is same with that of test, but the value of simulation is a little larger. The reason may be that the parameters of the electric motor by estimation are a little different from the realistic parameters.

In Fig. 11, the comparison is given between the simulating and testing result of the input torque of the parallel-axis gear reducer in time and frequency domain. Figure 11a, b gives the simulating and testing results in time domain. After the shock load is acted, the input torque of the parallel-axis gear reducer increases, and decreases when the shock load is over. The variation of the simulating result is same with the testing result, but the fluctuation of the simulation is larger. Figure 11c, d gives the frequency spectrums of the simulat-

Table 1 The parameters for simulation

Parameter	Value	Parameter	Value	Parameter	Value
J_m	0.0918 kgm ²	k_{t23}	8.2×10^5 Nm/rad	r_{br}	0.1316 m
J_1	0.0045 kgm ²	c_{t23}	0	r_{bpn}	0.0493 m
J_2	0.0032 kgm ²	k_{t4p}	1.6×10^5 Nm/rad	r_c	0.0875 m
J_3	0.0003 kgm ²	c_{t4p}	$21.1 \text{ N} \cdot \text{m} \cdot \text{s} \cdot \text{rad}^{-1}$	η_{14}	0.955
J_4	0.0472 kgm ²	k_{tpd}	1.35×10^6 Nm/rad	η_{sd}	0.978
J_d	30 kgm ²	c_{tpd}	0	α_s	22.95°
J_s	0.1054 kgm ²	$k_{\theta r}$	5.8×10^8 Nm/rad	α_r	20°
J_r	0.1906 kgm ²	r_{b1}	0.0211 m	R_s	0.1846 Ω
J_c	0.5747 kgm ²	r_{b2}	0.0518 m	R_r	0.2153 Ω
J_{pn}	0.0070 kgm ²	r_{b3}	0.0245 m	L_s	0.0018 H
k_{tm1}	1.3×10^4 Nm/rad	r_{b4}	0.0775 m	L_r	0.0018 H
c_{tm1}	$0.996 \text{ N} \cdot \text{m} \cdot \text{s} \cdot \text{rad}^{-1}$	r_{bs}	0.0312 m	L_m	0.0653 H

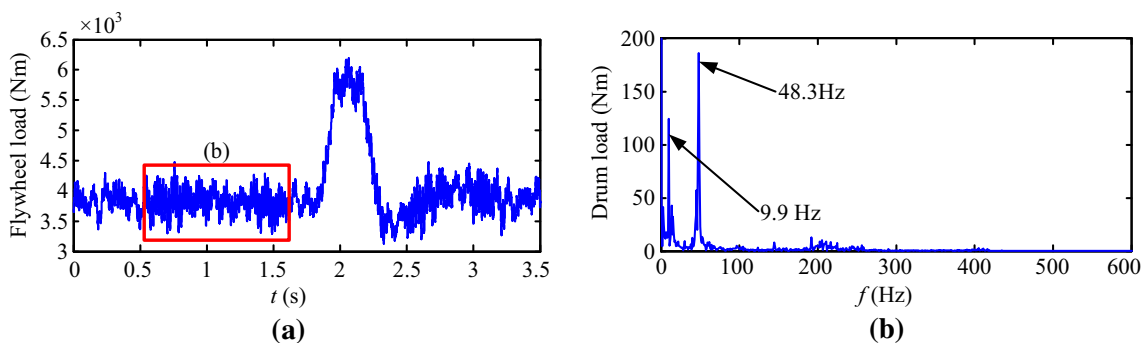


Fig. 9 The shock flywheel load for simulation which is obtained from the test

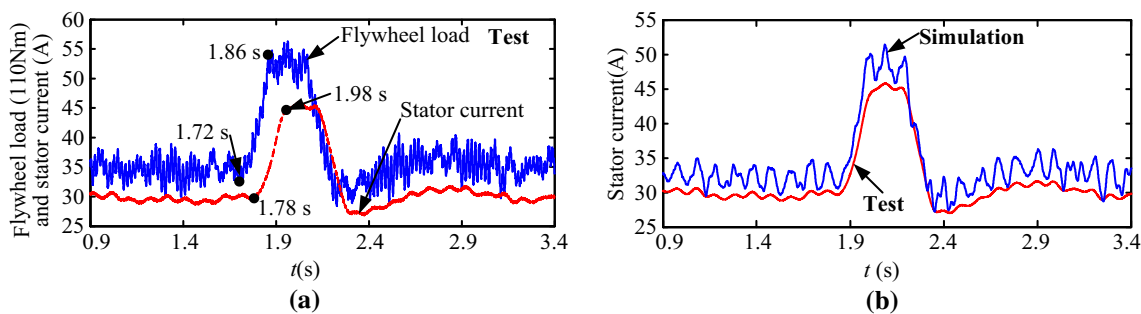


Fig. 10 The current characteristics of test and simulation

ing and testing result of the input torque of the parallel-axis gear reducer in stable period (the period in circle as shown in Fig. 11). The frequency components of the simulating result are same with the testing result. However, at some frequencies (for example, at 188.7 Hz), the amplitudes of the simulation are larger. The reason may be that the viscous damping model and its value have a little deviation from the realistic damping, leading to some frequency not being suppressed effectively. At high frequency (≥ 900 Hz), the amplitude of simulation is also larger. The reason may be that the meshing stiffness in simulation is suddenly changed

at the alternation of one and two gear teeth, inducing some components of high frequency, while in realistic conditions, the meshing stiffness is not suddenly changed. In Fig. 12, the comparison is given between the simulating and testing result of the input torque of the planetary gear reducer in time and frequency domain, from the this figure, the similar conclusion can be obtained with Fig. 11.

From Figs. 11 and 12, we can see a frequency component of 30 Hz is redundant in simulating results compared with testing results. To find the probable reason of this phenomenon, the simulating frequency spectrums are given in

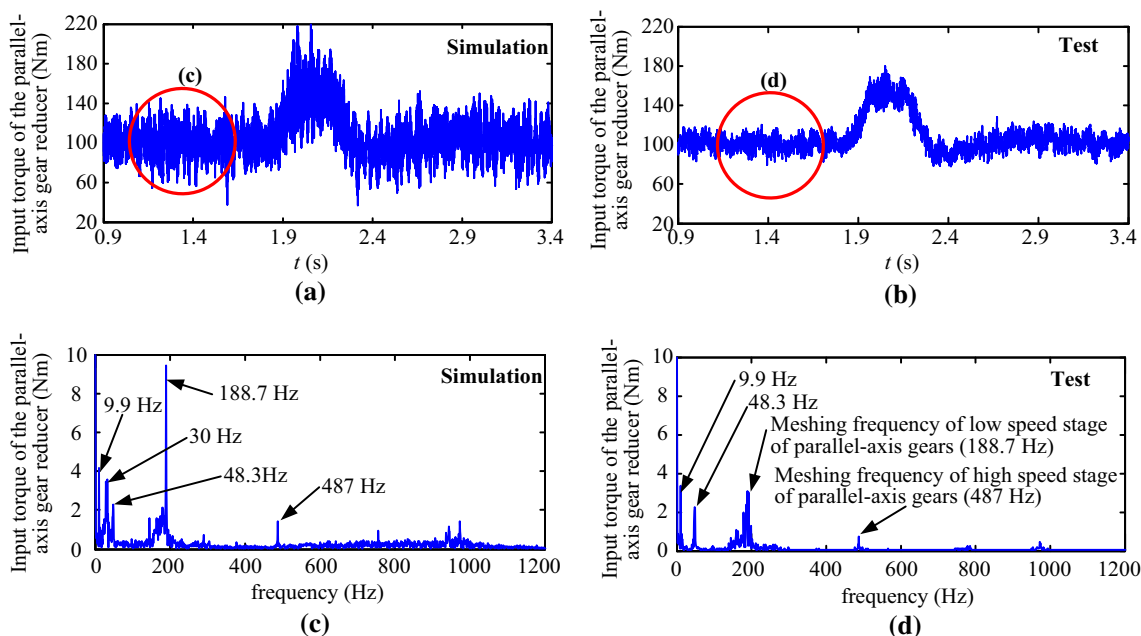


Fig. 11 Comparison between the simulating and testing result of the input torque of the parallel-axis gear reducer in time and frequency (stable) domain under shock load

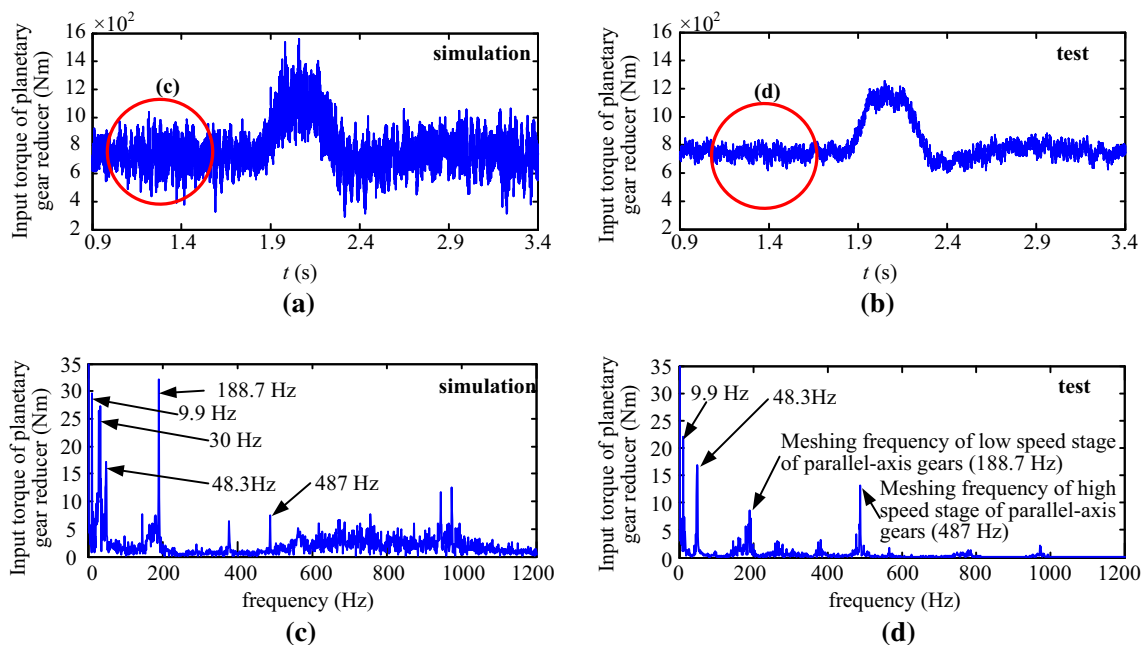


Fig. 12 Comparison between the simulating and measuring result of the input torque of the planetary gear reducer in time and frequency (stable) domain under shock load

Fig. 13 for the input torque of the parallel-axis gear reducer and planetary gear reducer when time-invariant meshing stiffness is used. The meshing frequency can be removed when the time-invariant meshing stiffness is used, however, the frequency component of 30 Hz still exists, and just the amplitude is smaller than that in Figs. 11 and 12 where the time-variant meshing stiffness is used. The program to reduce

the ripple of electromagnetic torque is usually contained in the realistic converter produced by ABB, but the algorithm is unknown for common user like us. Therefore, the program to reduce the ripple of electromagnetic torque is not contained in the converter model in the simulation. It is inferred that the redundant frequency component of 30 Hz in simulating results is the results of interaction of the ripple of

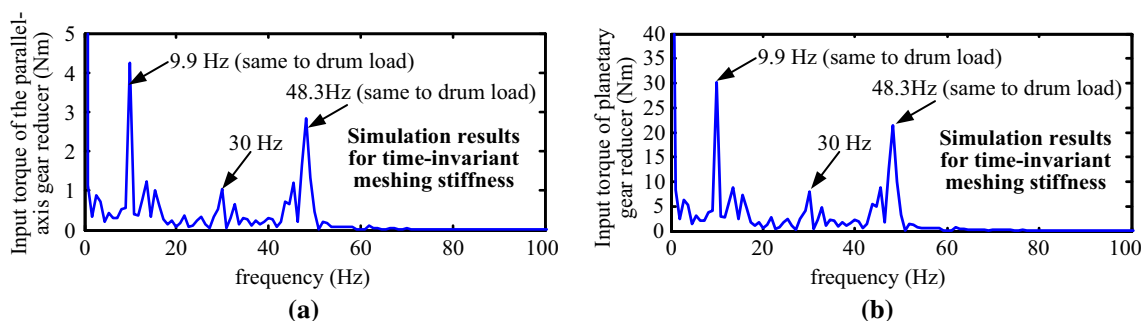


Fig. 13 The simulating frequency spectrums of the input torque of the parallel-axis gear reducer (a) and planetary gear reducer (b) when time-invariant meshing stiffness is used

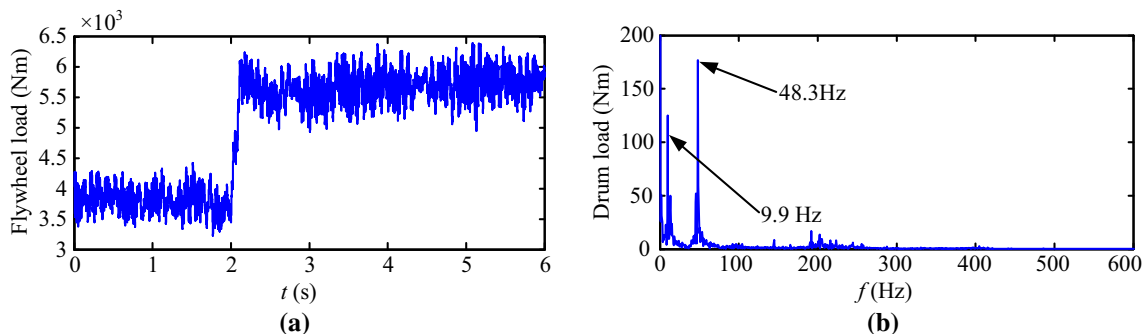


Fig. 14 The step flywheel load for simulation which is obtained from the test

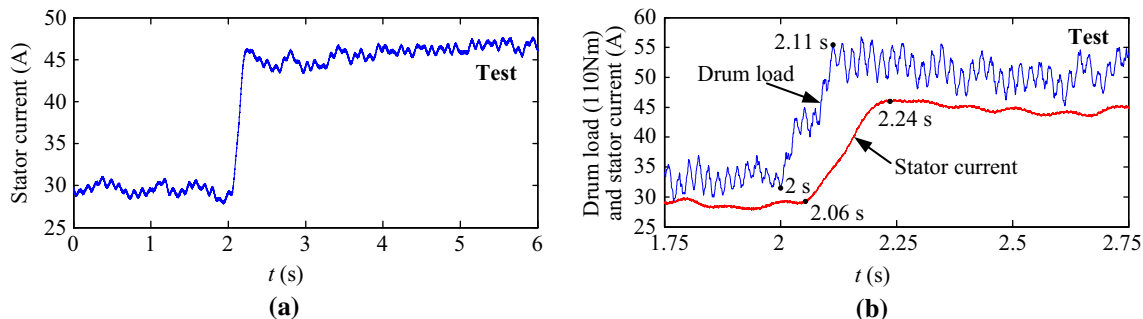


Fig. 15 Stator current of test (a) and comparison between flywheel load and stator current (b)

electromagnetic torque and time-variant meshing stiffness. So, to conduct the electromechanical dynamic analysis precisely, the cooperation of electrical engineer and mechanical Engineer is needed. The same phenomenon also exists in the results under step load in the Sect. 4.2.

The summary can be made for simulating and experimental investigation of electromechanical characteristics under the shock load as following: after the shock load being acted, the stator current and internal load of the transmission system increase, and decreases when the shock load is over; The stator current can reflect the shock flywheel load but with a little delay, so the stator current can be acted as the feedback signal to reflect the flywheel load, while the delay should be paid attention to; The electromechanical dynamic model can reflect the real system basically; The trend of simulating cur-

rent and internal load are coincided with the test results, but the amplitudes are a little larger for the simulating result.

4.2 Investigation under the step load

The step flywheel load is shown in Fig. 14, which is obtained from the measuring results of torque/speed transducer 3. The flywheel load at stable period contains two frequency components of 9.9 Hz and 48.3 Hz as shown in Fig. 14b. At the beginning of the simulation, it is the transient process, so the simulating result of 0.5 ~ 6 s is chosen to be compared with the test result.

The current characteristics of test are given in Fig. 15. In Fig. 15a, the stator current of test are given. After the shock load is acted, the stator current increases. In Fig. 15b,

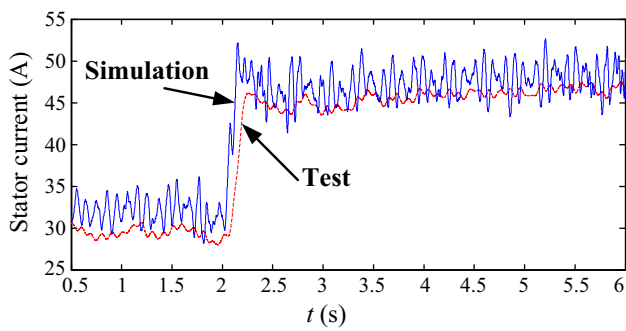


Fig. 16 Comparison between stator currents of test and simulation

the flywheel load and stator current of test are compared in time domain. The stator can reflect the sudden change of the flywheel load but with a little delay. In Fig. 16, the stator currents of test and simulation are compared in time domain. For clarification of the illustration, the stator currents are low-pass filtered with cutting frequency of 20 Hz. The variation trend of the stator current of simulation is same with that of test, but the value of simulation is a little larger. The reason may be that the parameters of the electric motor by estimation are a little different from the realistic parameters.

In Fig. 17, the comparison is given between the simulating and testing result of the input torque of the parallel-axis gear reducer in time and frequency domain. Figure 17a, b give the simulating and testing results in time domain. After the step load is acted, the input torque of the parallel-axis gear reducer increases. The variation of the simulating result is

same with the testing result, but the fluctuation of the simulation is larger. Figure 17c, d give the frequency spectrums of the simulating and testing result of the input torque of the parallel-axis gear reducer before and after step load. The frequency components of the simulating result are same with the testing result. However, at some frequency (for example, at 188.7 Hz), the amplitude of the simulation is larger. The frequency components don't change before and after step load, but the amplitudes increase after step load, for both the simulating and testing results. In Fig. 18, the comparison is given between the simulating and testing result of the input torque of the planetary gear reducer in time and frequency domain, from the this figure, the similar conclusion can be obtained to Fig. 17.

The summary can also be made for simulating and experimental investigation of electromechanical characteristics under the step load as following: After the step load is acted, the stator current and internal load of the transmission system increases; The stator current can reflect the step flywheel load but with a little delay, so the stator current can be acted as the feedback signal to reflect the flywheel load, while the delay should be paid attention to; The electromechanical dynamic model can reflect the real system basically under step load; The trend of simulating current and internal load are coincided with the test results, but the amplitudes are a little larger for the simulating result; The frequency components don't change before and after step load, but the amplitudes increase after step load.

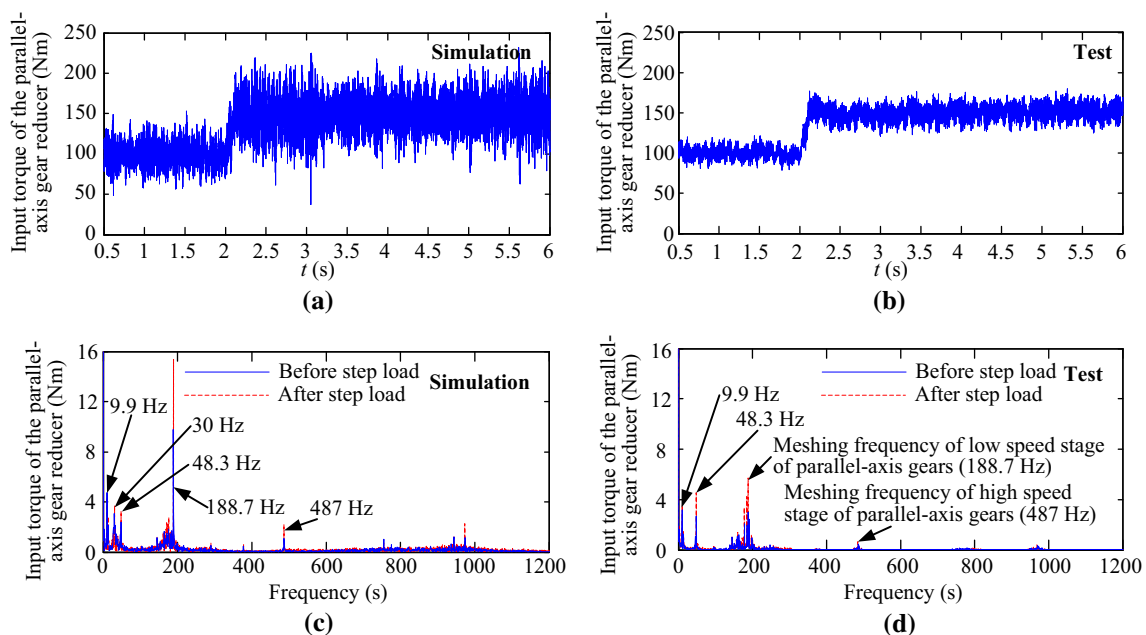


Fig. 17 Comparison between the simulating and testing result of the input torque of the parallel-axis gear reducer in time and frequency (stable) domain under step load

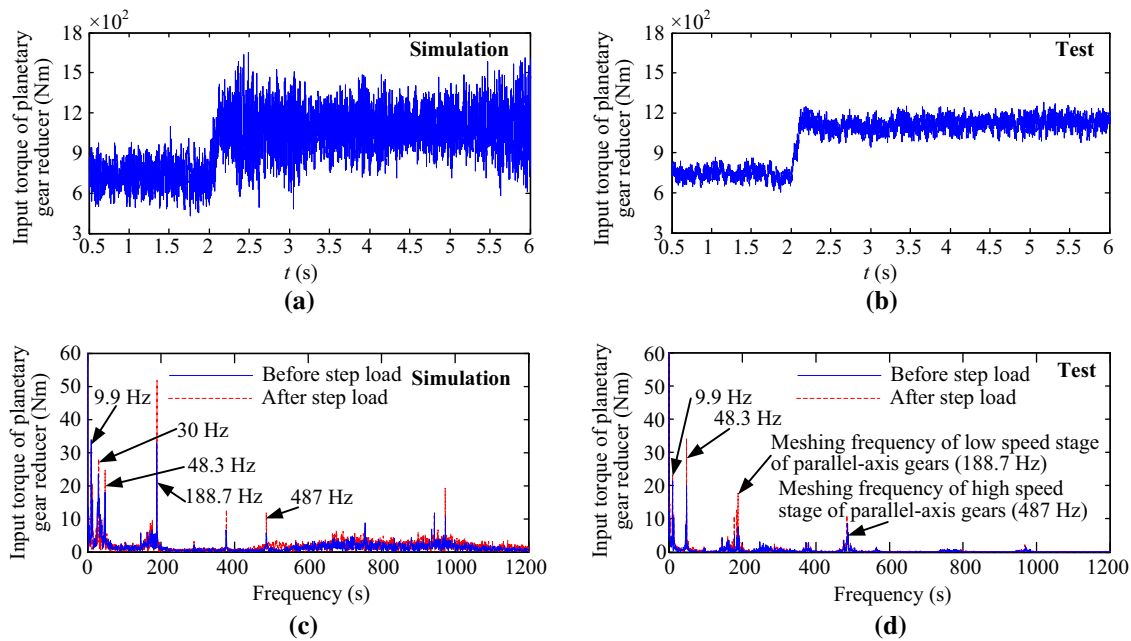


Fig. 18 Comparison between the simulating and testing result of the input torque of the planetary gear reducer in time and frequency (stable) domain under step load

5 Conclusion

A test rig is constructed for the multi-stage gear transmission system with planetary gears firstly. Then, the electromechanical dynamic model is constructed for the multi-stage gear transmission system. The electromechanical dynamic characteristics of the multi-stage gear transmission system are investigated by simulation and experiment under sudden-changing load to provide some guidance for improving the dynamic performance and monitoring the working state. The electromechanical dynamic modeling method is also validated by comparison between the experimental and simulating results. Based on these investigations, the following conclusion can be obtained.

- (1) The stator current and the internal load of the cutting transmission system increase or decrease as the flywheel load increases or decreases. The stator current (RMS) can reflect the sudden-changing flywheel load but with a little delay, so the stator current can be acted as the feedback signal to reflect the flywheel load, while the delay should be paid attention to.
- (2) The electromechanical dynamic model can reflect the real system basically under the sudden-changing load. The trends of simulating current and internal load are coincided with the test results in time and frequency domain, except that the amplitudes are a little larger for the simulating result, proving that the electromechanical dynamic modeling method herein is valid.

Acknowledgements The research is supported by National Natural Science Foundation of China (Grant No. 51705042), Sichuan Provincial Key Lab of Process Equipment and Control (Grant No. GK201713), the Fundamental Research Funds for the Central Universities (Grant No. 106112017CDJXY330001), and State Key Laboratory of Mechanical Transmission (Grant No. SKLMT-ZZKT-2017Z07).

References

1. Takahashi, I., Noguchi, N.: A new quick-response and high-efficiency control strategy of an induction motor. *IEEE Trans. Ind. Appl.* **22**(5), 820–827 (1986)
2. He, S., Gunda, R., Singh, R.: Effect of sliding friction on the dynamics of spur gear pair with realistic time-varying stiffness. *J. Sound Vib.* **301**(3–5), 927–949 (2007)
3. Velex, P., Sainsot, P.: An analytical study of tooth friction excitations in errorless spur and helical gears. *Mech. Mach. Theory* **37**(7), 641–658 (2002)
4. Velex, P., Maatar, M.: A mathematical model for analyzing the influence of shape deviations and mounting errors on gear dynamic behaviour. *J. Sound. Vib.* **191**(5), 629–660 (1996)
5. Kahraman, A.: Natural modes of planetary gear trains. *J. Sound. Vib.* **173**(1), 125–130 (1994)
6. Lin, J., Parker, R.G.: Analytical characterization of the unique properties of planetary gear free vibration. *J. Vib. Acoust.* **121**(3), 316–321 (1999)
7. Guo, Y., Parker, R.G.: Dynamic modeling and analysis of a spur planetary gear involving tooth wedging and bearing clearance non-linearity. *Eur. J. Mech. A* **29**(6), 1022–1033 (2010)
8. Kim, W., Lee, J.Y., Chung, J.: Dynamic analysis for a planetary gear with time-varying pressure angles and contact ratios. *J. Sound Vib.* **331**(4), 883–901 (2012)
9. Liu, C., Qin, D., Liao, Y.: Dynamic model of variable speed process for herringbone gears including friction calculated by variable friction coefficient. *J. Mech. Des.* **136**(4), 41001–41006 (2014)

10. Liu, C., Qin, D., Liao, Y.: Electromechanical dynamic analysis for the drum driving system of the long-wall shearer. *Adv. Mech. Eng.* **7**(10), 1–14 (2015)
11. Liu, C., Qin, D., Lim, T.C., Liao, Y.: Dynamic characteristics of the herringbone planetary gear set during the variable speed process. *J Sound Vib.* **333**(24), 6498–6515 (2014)
12. Chaari, F., Abbes, M.S., Rueda, F.V., Rincon, A.F.D., Haddar, M.: Analysis of planetary gear transmission in non-stationary operations. *Front. Mech. Eng.* **8**(1), 88–94 (2013)
13. Theodossiades, S., Natsiavas, S.: Periodic and chaotic dynamics of motor-driven gear-pair systems with backlash. *Chaos Solitons Fractals* **12**(13), 2427–2440 (2001)
14. Khabou, M.T., Bouchaala, N., Chaari, F., Fakhfakh, T., Haddar, M.: Study of a spur gear dynamic behavior in transient regime. *Mech. Syst. Signal Process.* **25**(8), 3089–3101 (2011)
15. Bartelmus, W.: Mathematical modelling and computer simulations as an aid to gearbox diagnostics. *Mech. Syst. Signal Process.* **15**(5), 855–871 (2001)
16. Feki, N., Clerc, G., Velex, P.: An integrated electro-mechanical model of motor-gear units—Applications to tooth fault detection by electric measurements. *Mech. Syst. Signal Process.* **29**, 377–390 (2012)
17. Mezyk, A.: Minimization of transient forces in an electro-mechanical system. *Struct. Optim.* **8**(4), 251–256 (1994)
18. Clerc, G., Feki, N., Velex, P.: Modeling of gear-motor dynamic interactions—applications to the detection of tooth faults by electric measurements. *VDI-berichte. 2108. Munich*, pp. 941–953 (2010)
19. Sika, G., Velex, P.: Analytical and numerical dynamic analysis of gears in the presence of engine acyclism. *J. Mech. Des.* **130**(12), 124501–124502 (2008)
20. Sika, G., Velex, P.: Instability analysis in oscillators with velocity-modulated time-varying stiffness—Applications to gears submitted to engine speed fluctuations. *J. Sound Vib.* **318**(1–2), 166–175 (2008)
21. Li, S., Kahraman, A.: A spur gear mesh interface damping model based on elastohydrodynamic contact behaviour. *Int. J. Powertrains* **1**(1), 4–21 (2011)
22. Shi, Z., Lim, T.C.: Effect of Hertzian impact damping on hypoid gear dynamic response. In: Velex P, edito. *International Gear Conference 2014: 26th–28th August 2014, Lyon*. Oxford: Chandos Publishing, 2014. pp. 1011–1019
23. Guilbault, R., Lalonde, S., Thomas, M.: Nonlinear damping calculation in cylindrical gear dynamic modeling. *J. Sound. Vib.* **331**(9), 2110–2128 (2012)



Changzhao Liu received Ph.D. degree in Mechanical Engineering from Chongqing University, Chongqing, China, in 2016. Now he works at Chongqing University as a lecturer. His current research interests include electromechanical dynamic of transmission systems.



Yinghua Liao is a Ph.D. Candidate in Chongqing University, Chongqing, P. R. China. Now he works at Sichuan University of Science and Engineering, Zigong Sichuan, P. R. China. His current research interests include dynamics and reliability of mechanical systems.



Yong Wang is a Ph.D. in Chongqing University, Chongqing, P. R. China. Now he works at Chongqing College of Electronic Engineering, Chong Qing, P. R. China. His current scientific interests include automotive automatic transmission system design theory and method of controlling.